Monitoring concrete frames with brick walls using photogrammetry

Filipa Borges Marques

October 2016

Abstract

Structural monitoring allows to promptly detect possible structural faults, enabling their correction and stopping their evolution. It also allows the correct understanding of the structural response when subjected to loading. Usually, monitoring is performed by traditional methods that implies, after a visual inspection, the application of non-destructive tests and equipment to measure displacements and deformations. These methods show several drawbacks, such as being time-consuming, expensive and limited by the devices available. Moreover, they are only capable of monitoring critical sections on a limited number of pre-defined points.

In order to overcome those disadvantages, methods based on image processing and photogrammetry have been developed. The chronological analysis of sets of imagens, from structures or structural members, enables a more efficient assessment.

In the present study, a method based on photogrammetry and post-processing of acquired data was used to monitor experimental tests on reinforced concrete frame, with and without masonry wall. The proposed method allows a complete and discrete characterization of the deformed shape evolution, compute displacement and strain fields and the principal strains directions. The main advantage of the method is the quantity and quality of the information attained, through a single acquisition system. The outputs obtained allow to evaluate other relevant parameters to the structural analysis, namely, identification of the diagonal of compression and cracking regions. Finally, it is quite important to point out that the method assists a complete understanding of the structural response up to failure in a precise and efficient way.

Key-words

Photogrammetry; Post-Processing; Monitoring; Deformation; Concrete; Robustness.

1 Introduction

The minimization of structural interventions during the lifetime of buildings implies their correct monitoring. The goal of this monitoring is to timely detect possible structural failures, allowing their corrections and thus stopping the deterioration of the structures.

Usually, structural monitoring, in constructions in service or in laboratorial tests, is carried out applying traditional methods such as visual inspections and applying non-destructive testing in critical sections. Displacements and deformations are assessed with LVDTs and strain gauges.

Some of the new methods that have arisen rely on image processing techniques and photogrammetry. In fact, the analysis of sets of images chronologically ordered of structures or structural members, allows to detect anomalies and efficiently perform a structure analysis, allowing the calculation of displacement, deformation and strain fields, amongst other measurements that help understand, predict and/or confirm their behaviour.

The experimental test analysed was carried out on the scope of the project “ROBUST BRICK – Use of masonry in improving structural robustness of

buildings" (PTDC/ECM-COM/2911/2012), financed by the Fundação para a Ciência e Tecnologia, whose objective was to evaluate the contribution of non-structural masonry walls on the safety of buildings after an unpredictable event.

This work aims to implement and evaluate a method for monitoring this tests in reinforcement concrete frames, based upon photogrammetry and post-processing of the collected data, as a way of allowing a more detailed structural analysis of the frame. The following goals may also be established: (i) the definition of the global deformed shape on several key-instants of the tests; (ii) the determination of the displacement field in zones of beam-to-column connections; (iii) the estimation of the strain field in zones of beam-to-column connections.

2 Structural Monitoring Based on Vision Systems

2.1 Framework

The monitoring of structures is essential for the correct diagnosis of their state of conservation and/or to assess, in a detailed manner, their behaviour in experimental tests. It can supports the execution control, evaluates the structural safety and follows the entire lifetime of a structure. It also presents great potential and enables a detailed understanding of its behaviour, so that can efficiently act in conformity. This is vital to any kind of structure, since it helps predict its performance, hence allowing the timely detection of degradation processes and the mitigation of their effects and, therefore, extending the lifetime of the structures.

2.2 Vision Systems

Artificial vision systems try to replicate the human visual system through algorithms; they rely upon the use of photographic or video cameras and in image analysis algorithms. Artificial vision can be used as a structural monitoring system, in a quasi-continuous way or through the acquisition of temporal records on selected targets [5].

All these systems present two major stages: the image acquisition and the analysis and processing of images (using software specifically developed with this purpose).

Some of the techniques applied to the analysis of the images are photogrammetry and the digital image processing. These procedures allow to attain important information about the objects portrayed in the images, allowing detection, identification, geometrical characterization, enhancement and segmentation.

Photogrammetry is a technique used to obtain reliable and accurate geometrical information about physical objects [9] through a process of recording, measuring and interpretation of photographical images [6]. In order to calculate the displacement fields, several natural or artificial targets may be used. Natural targets are objects already present in the images, such as lamps or street signs; on the other hand, artificial targets are painted on the desired structure.

Digital Image Processing is the process of transforming a digital image into another one with more desirable properties, such as reduce noise, less geometrical distortion, greater sharpness, amongst other transformations [4], using a computer.

The fields of application of the referenced techniques are vast. In civil engineering, the main goal is focused in follow the evolution of displacement in buildings and structural members, to compute deformations, and to define cracking patterns. They can be undertaken both in service (real) structures as well as in laboratorial tests.

3 Monitoring Systems Using Photogrammetry

3.1 Test Set-up

The reinforced concrete frame was design according to the Eurocode 2 (Eurocode-2, 2010), and it had the following dimensions (values measured between the axis of the elements): 5000mm × 2550 mm (Figure 1). The concrete presented a mean compressive strength of 44.23 MPa and the steel presented a mean tensile strength of 540 MPa and an elasticity modulus of 200 MPa.

The masonry wall was made of a double panel with an air gap of 40 mm and had continuous joints. The

bricks used on the wall were 300 × 200 × 150 mm^3 and 300 × 200 × 110 mm^3, with average compressive strength of 2.5 MPa, average tensile strength of 0.27 MPa and an elasticity modulus of 6.55 MPa. The following nomenclature for the structural elements was defined as follows: V1 and V2 for the superior and inferior beam, and P1 and P2 for the left and right columns, respectively.

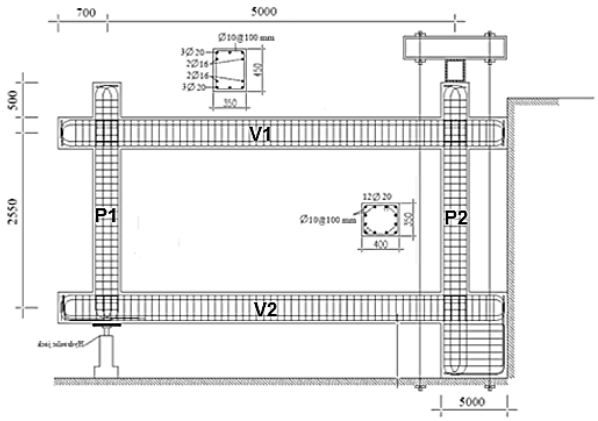

Figure 1– Frame Dimensions (Baghi,2006).

The test consisted on applying an ascending vertical load, using a hydraulic hammer placed on the inferior face of the beam V2, on the section of beam- column connection. This same section was also monitored with a load cell and an LVDT.

The structure was overdesign to be tested with and without the masonry wall. During test 1.1 (Figure 2) and 1.4 (Figure 5) only the behaviour of the frame was examined. During test 1.2 (Figure 3) the frame with the masonry wall was tested and during test 1.3 (Figure 4) the frame with a previously strengthened masonry wall was studied. To each test, a different analysis was carried out, namely (Graph 1):

1.1 – elastic analysis without masonry wall;

1.2 – elastic analysis with masonry wall;

1.3 – elastic analysis with strengthened masonry wall;

1.4 – failure analysis of the frame.

Figure 2 – Test 1.1.

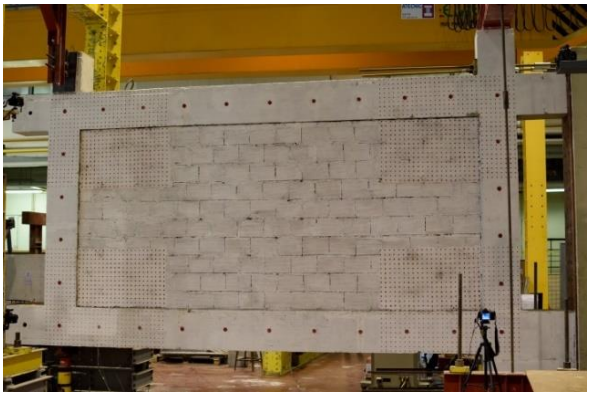

Figure 3 - Test 1.2.

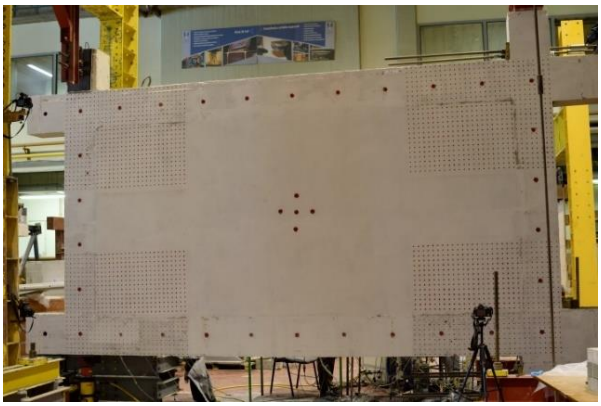

Figure 4 - Test 1.3.

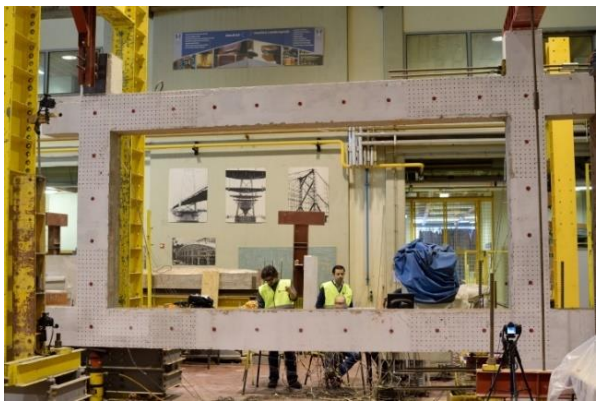

Figure 5 - Test 1.4.

Graph 1 shows the load-displacement curves of the 4 referenced tests. The marked points over the

curves show the instants of the test analysed by photogrammetry.

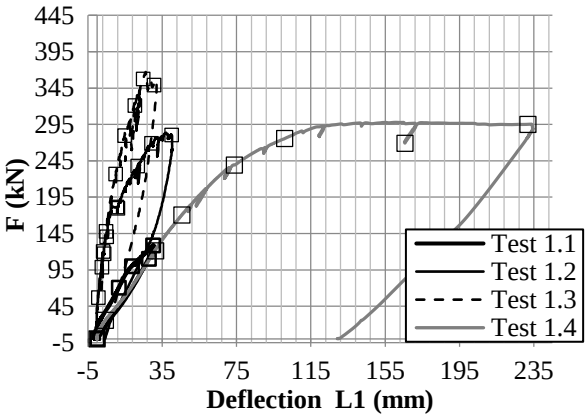

Graph 1 - Load vs displacement curve.

3.2 Procedure

The frame was monitored with 5 photographic stations: a general one and four local stations. The general station was used to calculate the deformed shapes of the frame, and the field of vision covered the whole structure. The local stations were placed on the beam- column connections, allowing the detailed calculation of the displacement and strain fields. All the algorithms and routines used were previously developed and implemented in MatLab (Matlab R2015a).

3.2.1 Frame Preparation

The surface of the frame was painted white, with the goal of simplifying the detection of targets on the picture. Several sets of circular targets were painted red, aiming to create a high contrast. In order to carry out a global analysis of the frame, 30 targets measuring 50 mm in diameter were painted, spaced by 500 mm (Figure 6).

To the local analysis of the of corners (zone of beam-column connection), a regular grid of circular targets, measuring 10 mm in diameter, was painted, spaced of 50 mm, in a rectangular 1450 mm × 1100 mm area.

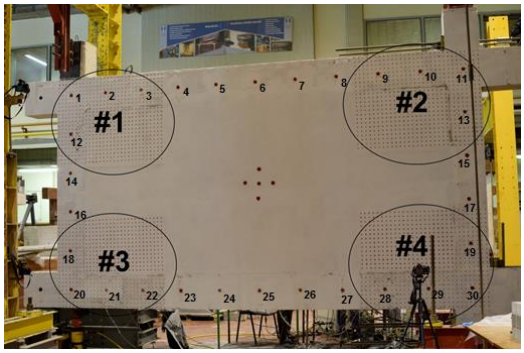

Figure 6 - Numbering of the stations and targets.

3.2.2 Image Acquisition

For monitoring of the tests, images were simultaneously taken from the 5 referenced stations. The general station was denominated #5 while the local stations were numbered from #1 to #4, as it can be seen in Figure 6.

To maintain stability during the whole test, the photographic cameras were placed on tripods and remote triggers were used. The characteristics of the cameras used are registered on Table 1. The focusing was made before each test and was held constant during the test.

Table 1 - Photographical camera's characteristics.

Station	Camera	Resolution threshold (pixels)	Focal lenght (mm)
#1 e #3	D3000a-b	4608x3072	18
#2	D200	3872x2592	18
#4	D3000	3872x2592	18
#5	D5300	6000x4000	30

On test 1.2, 1.3 and 1.4, 10 pictures were attained immediately before the beginning of the test. The difference of coordinates in this instant, 'stage 0', was used as a measurement to estimate the precision of the detection algorithm.

The images are associated with a testing time, which is synchronized with the measuring time of the traditional instrumentation (LVDT, load cell and strain gauges).

3.2.3 Target Detection

The first step to detect the targets consists of measuring, in pixels, the approximated value of the diameter of the targets [8]. Posteriorly, it is selected

the area with the targets wished to be detected, and an algorithm based of the Hough transform is applied. The algorithm is capable of detecting targets which are not perfect circles, e.g. ellipses with similar semi-axis values [1].

For station #5, the centres of the 30 global targets are detected on the several stages of testing (Figure 7). The software detected the coordinates of the 30 global targets, in pixels.

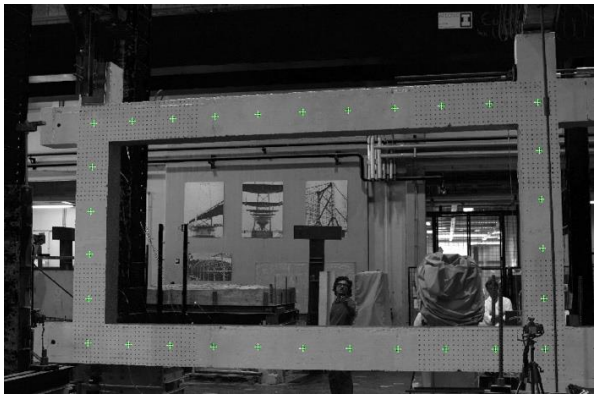

Figure 7 – Detection of the general targets - #5.

To the detection of the stations' #1, #2, #3 and #4 targets, the process used showed some differences, given that some images exhibited a great rotation between the plane of the frame and the plane of the picture and, thus, they were not detected by the algorithm. The global targets present on the pictures of the local stations were detected and so the coordinates of the global targets were obtained on the local images, in pixels.

3.2.4 Determination of the Homography and Orthorectification Matrix

Homography is a linear transformation which allows one to establish a correspondence between coordinates of points in the real world belonging to a plane and their projections on the picture [3].

The calculation of the homography matrix is carried out so that orthorectified images could be produced, that do not show distortion, making the coordinates more accurate and correcting perspective effects and the influence of embossment. An example of this transformation can be seen on Figure 8.

(a) (b)

Figure 8 – Test 1.2 #2 (a) Original image; (b) Orthorectified image.

3.2.5 Calculation of the Coordinates of the Targets in Millimetres.

Through the coordinates in pixels of the 30 global targets and the homography matrix, the coordinates of the 30 targets of the general station were calculated in millimetres.

With respect to the local stations, firstly the orthorectified images were produced. The software detected the coordinates of the local targets, in pixels that, using a scale factor, were transformed in millimetres. The number of detected targets varied according to the station and test analysed and are presented in Table 2.

Table 2 - Number of analysed targets.

Test/station	#1	#2	#3	#4
1.1	-	361	378	360
1.2	690	610	646	624
1.3	690	-	667	626
1.4	-	329	345	-

3.2.6 Characterization of the Deformed Shape:

The number of targets used on station #5, 30, allows to calculate the deformed shape of the frame with high discretization, the rotation of all the structural elements and the distortion of the frame, in beam- column connections.

In order for the deformed shape to be traced, the displacement of each target was computed, using the difference of coordinates, in millimetres, between the stage analysed and the initial stage.

3.2.7 Strain on the Concrete Surface

On the local stations (stations #1, #2, #3 and #4), the calculated displacement field, associated with an auxiliary triangular mesh, built upon the targets,

allowed the calculation of the strain on the surface for the several stages of the tests.

The calculation of the strain was made based on the following steps and suppositions: (1) definition of a mesh of triangular elements based on grid of targets, applying Delaunay triangulation [9]; (2) assuming an uniform deformation on the evaluated surface and applying a standard procedure of the Finite Elements Method to obtain elementary strains, ε^e [2]; (3) calculating the values of the nodal strains, ε^n, (Figure 9), taking in account the strain in every element (ε^e) that shared a node [7].

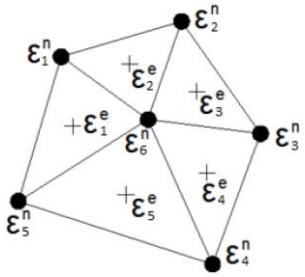

Figure 9 - Elementary strain (ε^e) e nodal strains (ε^n).

3.3 Estimation of the Error

The precision was considered as a measure to evaluate the error. This was calculated through the root mean square (RMS). This value arises from the differences of coordinates of the centres of the targets [9] and corresponds to que square root of the arithmetic mean of the square of the values.

The error of the strain field is presented in permillage and was calculated trough the following equation in which $l0$ is the mean distance between targets and $error\ \delta$ is the error associated with the displacements.

$$error\ \varepsilon = \frac{error\ \delta}{l0}$$

4 Results

4.1 Analysis of the Frame

In this subchapter, the results attained through the analysis of the general station are presented.

4.1.1 Region of Maximal Displacement

As expected, the region of maximo displacement occurs at column P1. To assess the possible existence of some gross error, the vertical displacements logged on target number 20 were compared to the values measured by the LVDT. Through analysis of Figure 10, one can verify that the deviation between the values measured by the LVDT and the values obtained by photogrammetry are not significant, being the mean difference of 1.10 mm.

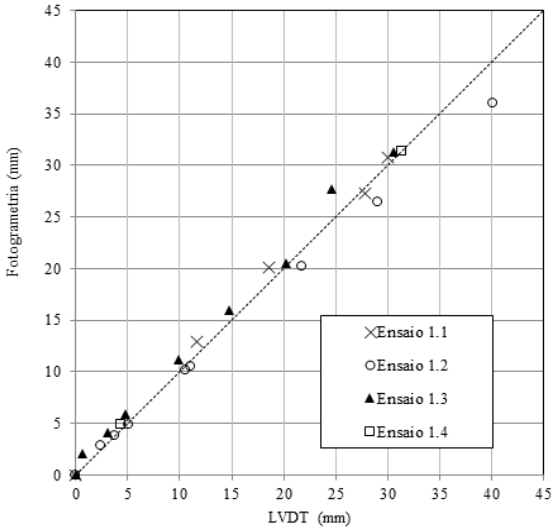

Figure 10 - Photogrammetry vs. LVDT in the section of load application in relation to measured displacement.

4.1.2 Deformed Shape

The configuration of the deformed shape was discretized attained, from the displacements measured in each of the 30 global targets. In the figures below, the layouts of the deformed shapes are shown, per stage and test: test 1.1 (Figure 11), test 1.2 (Figure 12), test 1.3 (Figure 13) and test 1.4 (Figure 14). In each of the tests, the deformed shapes were overlapped with the ortho-rectified image of the initial stage and its values (in millimetres) amplified.

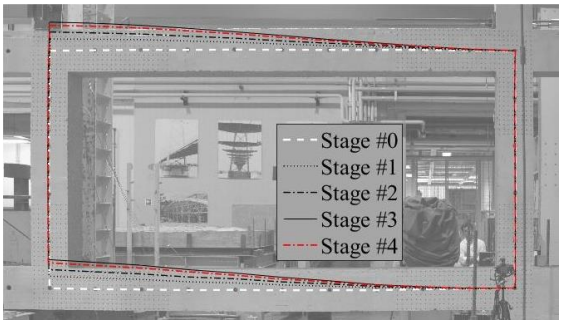

Figure 11 - Deformed shape test 1.1 (amplified x10).

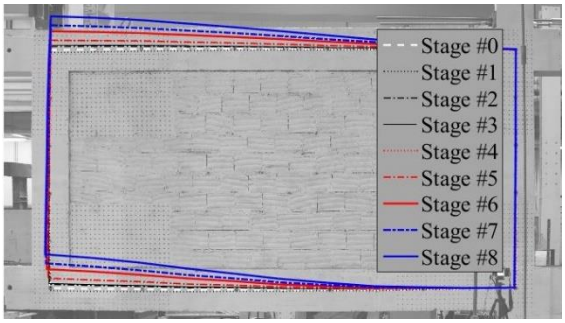

Figure 12 - Deformed shape test 1.2 (amplified x10).

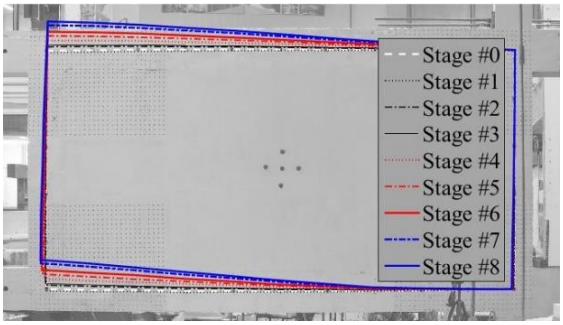

Figure 13 - Deformed shape test 1.3 (amplified x10).

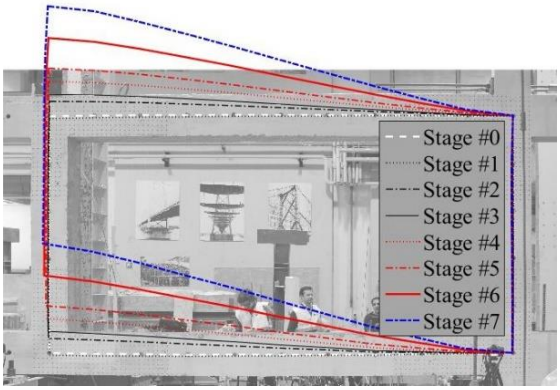

Figure 14 - Deformed shape test 1.4 (amplified x5).

Through visual assessment of the deformed shapes, it can be concluded that que columns did not show significant rotation in any of the tests, which can be explained by the fact that the load applied had a vertical direction and there was an almost complete fixed support. In tests 1.1, 1.2 and 1.3 the order of magnitude obtained for the displacements was similar, since they were all performed on the elastic regime. In the test 1.4 the displacements were greater because this was a failure test. The values of rotation for each structural element, relative to the last stage analysed of each test are shown in Table 3.

Table 3 - Values of maximal rotation per element.

	ϕ(º) – Rotation			
Test	**ϕV1**	**ϕP2**	**ϕV2**	**ϕP1**
1.1	3.13	0.03	3.09	0.31
1.2	4.03	0.39	4.05	1.40
1.3	3.48	0.73	3.55	1.76
1.4	25.07	0.33	24.69	2.43

The study of the deformed shapes (configuration of the deformed shape, displacement of targets and rotation of the four elements) allows one to verify that column P2 has an almost complete fixed support. Column P1 shows constant vertical displacement. The rotation of this member is due to the rotation of the beams and their support conditions. The behaviour of horizontal members, beams V1 and V2, is similar, i.e., both show the same value of rotation because the displacements at their ends are identical. Test 1.4 shows higher values for rotation and cracking is noticed on the frame, given that it is a failure test.

In regard to distortion, the values logged support the observation of the deformed shapes, where angle P2-V1 and angle P1-V2 grew and angles V1-P1 and V2-P2 decreases. In general, the sum of the distortions angles, in each test, tends to zero.

Table 4 - Values of distortion between elements.

	ΔϒV (º) – Distortion between elements			
Test	**ΔϒV V1-P1**	**ΔϒV P1-V2**	**ΔϒV V2-P2**	**ΔϒV P2-V1**
1.1	-2.82	2.78	-3.13	3.16
1.2	-2.63	2.65	-3.65	3.64
1.3	-1.72	1.79	-2.83	2.75
1.4	-22.65	22.26	-24.35	24.74

4.2 Analysis of the Beam-Column Connection

In this subchapter the results obtained through the analysis of local stations (stations #1, #2, #3, and #4) are presented.

4.2.1 Displacements Field

The displacements field show an identical direction and orientation on every test, being their magnitude the only variable; because of this, only the images

of the displacement vectors relative to test 1.2 (Figure 15) are shown.

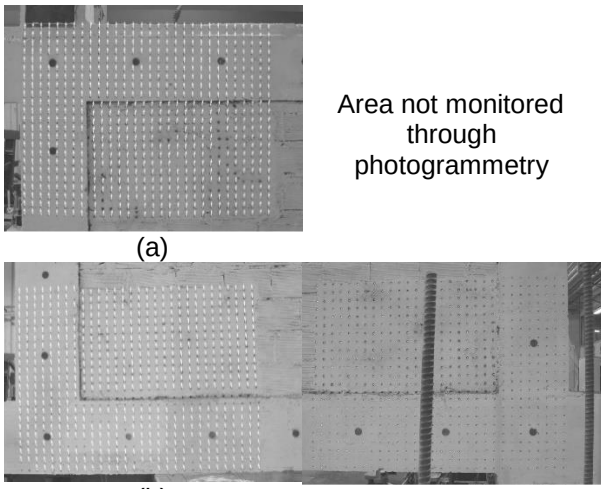

Figure 15 - Field of displacement during test 1.2, stage 8 (280,56kN) for: (a) station #1; (b) station #3; (c) station #4.

The values of maximum displacement are presented on Table 5. As it was expected, the values for the displacements, through analysis of station #1 and #3, to the same test, show similar magnitude, because they measure the displacement of the same column. The values calculated from the analysis of station #5 are on the same order of magnitude as the previous.

Table 5 - Maximal values of displacement obtained through photogrammetry.

Test	Maximal Displacement (mm)				
	#1	#2	#3	#4	#5
1.1	-	5.6016	27.8069	4.0743	27.6192
1.2	37.3319	11.8082	36.2600	-	36.4788
1.3	32.3347	-	31.9935	-	28.1005
1.4	-	50.8138	166.7868	-	168.7607

Later, the stages of each test were selected and the values of displacement for identical levels of load (~120 kN) were compared.

Table 6 - Values of displacement for the stage F≈120kN.

Test	Displacement F≈120kN (mm)				
	#1	#2	#3	#4	Force (kN)
1.1	-	6.12	31.32	4.67	128.80
1.2	4.05	0.59	3.84	0.84	117.07
1.3	4.20	-	4.27	10.33	120.50
1.4	-	6.45	31.72	-	121.08

4.2.2 Strain Fields

The principal strains fields were computed based on the displacement fields of the local stations. Two maps were drawn for each of the analysed stages in each test: a map of maximal principal strain (ε1); and another map of minimal principal strains (ε3). Both shows also the respectively principal directions, represented by black lines, calculated and drawn for each target.

The global behaviour of the frame was similar in every test so only the minimal strain field calculated on the final stage of test 1.2 (related to compressions) (ε3) is shown on Figure 16.

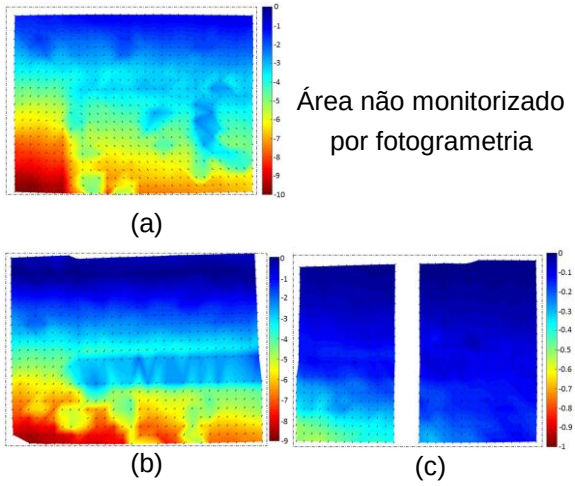

Figure 16 - Minimal principal strain (ε3) during test 1.2, stage 8 (280,56 kN): (a) station #1; (b) station #3; (c) station #4.

These maps allow to confirm that the force was distributed by the beam V2 and the column P1. The values of compression gradually diminish as column P2 is approached. The maps also permit the identification of the path of the loads and of the direction of the diagonal of compression.

Observation of Figure 17 leads to the conclusion that the strain on the surface of the concrete increases with the increase of load. It is seen that

the increase of compression is distributed, mainly in the beam V2.

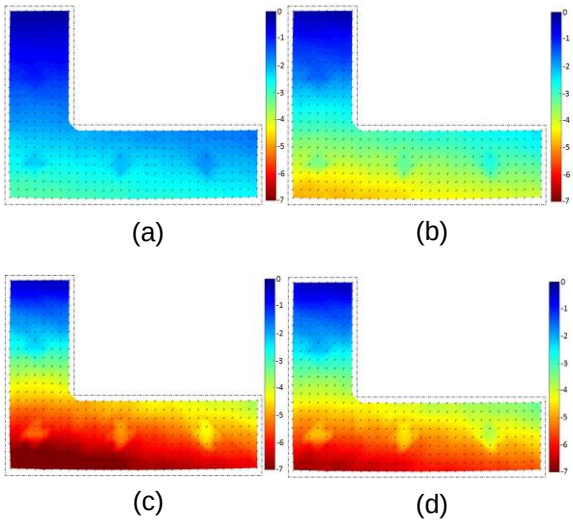

Figure 17 - Minimal principal strain (ε3) during test 1.1: (a) Stage1 (70,59kN); (b) Stage 2 (100,13kN); (c) Stage 3 (128,80kN); (d) Stage 4 (109,97kN).

The principal directions (of minimal strain), allow the identification of the position where the inversion of the deformed shape is located, i.e, the points where the lines (that represent principal direction) change direction.

At the end of the test, the opening of a small crack is noticed. This crack appears perpendicularly to the principal directions of the maximum principal strain and, as a consequence, in parallel to the directions of minimal principal strain.

Trough analysis of test 1.2, station #3 (Figure 18), one can conclude that on initial stages, the force is transmitted to the frame and is distributed equally through the column, the beam and the masonry wall.

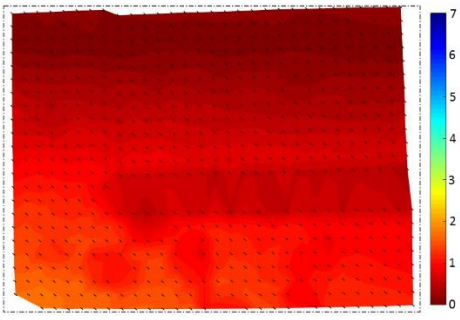

Figure 18 - Test 1.2 – Stage 5- ε1.

In stage 6, the opening of a crack and the separation of the masonry wall from the inferior beam is noticed (Figure 19). After the detachment of the wall from the beam, only the last one transmits the load.

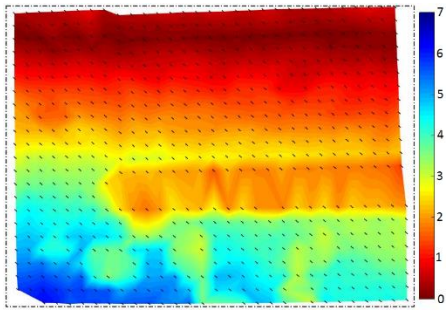

Figure 19 - Test 1.2 – Stage 8 - ε1.

The test 1.3 shows that, the wall reinforcement the structure worked properly, as before the damage. It can be conclude that the wall behaves as expected (Figure 20(a)) until a new crack and a new detachment between wall and frame arises (Figure 20(b)).

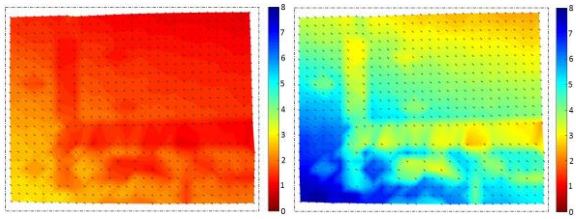

Figure 20 - Maximal principal strain (ε1) during Test 1.3: (a) Stage 4 (226,85kN); (b) Stage 7 (269,07kN).

Table 7 shows the values of maximal and minimal principal strains for the last stage of each test.

Table 7 - Maximal and minimal strains.

	Strain (‰)	
Test	**Maximal**	**Minimal**
1.1	5.76	-6.75
1.2	6.16	-8.80
1.3	7.89	-13.17
1.4	54.26	-64.04

The values of strain presented, that correspond to the values of strain on the concrete's surface, are higher in comparison to the characteristic value for the concrete strain ($\varepsilon_{concrete}$=2,5‰) which means that they can only be useful for a qualitative evaluation of the structure's behaviour.

The method allows the detection of critical areas such as cracking zones and the identification of compression rods as well as their inclination.

4.3 Estimation of the Error

The accuracy was evaluated experimentally through RMS values. For tests 1.2, 1.3 and 1.4 the mean RMS values obtained vary between 0.035mm and 0.158 mm.

The error associated to the strains was calculated in permillage and vary between 0,70‰ and 1,76‰.

5 Conclusions

The proposed method allows a complete and discrete characterization of the deformed shape and of the displacement and strain fields of structures connections, being an efficient and precise tool. The outputs attained also allow the evaluation of other important parameters for structural analysis, namely, identification of diagonal of compression and cracking regions.

The method enables the evaluation of all parameters above mentions on a large number of points, only limited by the resolution of the image and the number of targets used. One major advantages of the method is the quantity of information that can be obtained through a single system of acquisition. The multi-station approach leads to a detailed monitoring of the connections.

In relation to traditional methods, the one based on photogrammetry shows the following advantages: non-contact procedure; the large amount and quality of data; low-cost application; fast preparation and processing.

In regard to draw the deformed shape, a relevant plus of the method is the discretization achieved, since there is no constrains in the number of targets to be used. The deformed shape can be properly characterized by the displacement of each point, the rotation of the structural members, and the distortion of the frame.

The method enables to compute the displacement and superficial strain fields on beam-column connections, through extremely elucidative maps: the direction and magnitude of nodal displacement can be visualized; the load path can be identified and characterized (inclination of the diagonal of compression); the cracking regions and direction of their opening can be defined.

Finally, it is important to stress that the method applied allows the complete and detailed understanding of the structural response of a structure with real dimensions. Although the test was carried in laboratorial environment, it was executed in real size structure until failure.

6 Bibliographic References

[1] Ballard D. *Generalizing the Hough Transform to Find Arbitrary Shapes*. Pattern Recognition. 1981;13:111–22. (1981).

[2] Botelho, M. H. C. *Resistência dos materiais para entender e gostar: um texto curricular*. Studio Nobel, (1998).

[3] Criminisi, A. *Single-view metrology*. Accurate Visual Metrology from Single and Multiple Uncalibrated Images. Springer London, (2001). 69-105.

[4] Marques F., Ogê, and Neto H. V. *Processamento digital de imagens*. Brasport, (1999).

[5] Silva, S., Bateira J., and Caetano E. *Sistema de Visão Artificial para Monitorização de Vibrações em Tirantes de Pontes*. Revista da Associação Portuguesa de Análise Experimental de Tensões ISSN1646: 7078 (2008).

[6] Slama, Chester C., Theurer C., and Henriksen S. W. *Manual of photogrammetry*. No. Ed. 4. American Society of photogrammetry, (1980).

[7] Soriano, Lima H., and Lima S. de S *Método de Elementos Finitos em Análise de Estruturas Vol. 48*. EdUSP, (2003).

[8] Valença, J., et al. *Automatic crack monitoring using photogrammetry and image processing.* Measurement 46.1 (2013): 433-441.

[9] Valença, J. *Monitorização do estado de conservação de estruturas de betão por processamento de imagem e análise multi-espectral*. (2011).